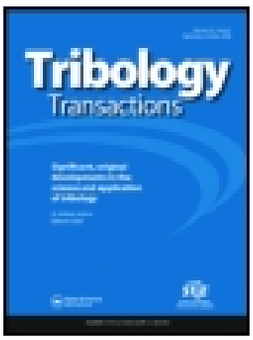

Tribology Transactions

ISSN: 1040-2004 (Print) 1547-397X (Online) Journal homepage: http://www.tandfonline.com/loi/utrb20

Material Transfer Behavior between a Blade and Two Types of Coating during High-Speed Rubbing

Weihai Xue, Siyang Gao, Deli Duan, Jiaping Zhang, Yang Liu & Shu Li

To cite this article: Weihai Xue, Siyang Gao, Deli Duan, Jiaping Zhang, Yang Liu & Shu Li (2018): Material Transfer Behavior between a Blade and Two Types of Coating during High-Speed Rubbing, Tribology Transactions, DOI: 10.1080/10402004.2018.1427292

To link to this article: https://doi.org/10.1080/10402004.2018.1427292

Accepted author version posted online: 23 Jan 2018.
Published online: 30 Apr 2018.

TRIBOLOGY TRANSACTIONS
https://doi.org/10.1080/10402004.2018.1427292

Material Transfer Behavior between a Blade and Two Types of Coating during High-Speed Rubbing

Weihai Xue[a], Siyang Gao[a], Deli Duan[a], Jiaping Zhang[b], Yang Liu[a], and Shu Li[a]

[a]Institute of Metal Research, Chinese Academy of Sciences, Shenyang, P. R. China; [b]Liming Aero-Engine Group Corporation, Shenyang, P. R. China

ABSTRACT

The material transfer behaviors of Al-hBN and NiAl-hBN coatings rubbed by a Ti6Al4 V blade at different linear speeds and single pass depths were studied using a high-speed rubbing tester. The blade height variation analysis, morphologies, energy-dispersive spectroscopy, and X-ray diffraction studies of the blade and the coating wear scars indicated that the coating material transferred to the blade during rubbing with the Al-hBN coating. For the NiAl-hBN coating, the blade material transferred to the coating. The temperature differences at the interface, varying melting points of the coatings, and blade plastic flow softening under high temperatures were regarded as factors for different material transfer behaviors.

ARTICLE HISTORY
Received 2 January 2017
Accepted 9 January 2018

KEYWORDS
Abradable seal coating; high-speed rubbing; material transfer; flash temperature

Introduction

To increase the efficiency and reduce the fuel consumption of aircraft turbine engines, the gaps between rotating and stationary parts, such as the clearance between the case and the blade, should be kept as small as possible. However, given the different thermal expansion coefficients of the case and the blade, along with blade elongation caused by high-speed rotation, a small reserved clearance can cause the blade to rub against the case, which seriously threatens engine security.

To guarantee flying safety and prevent the blade from rubbing against the case, an abradable seal coating is applied on the engine. This coating is sprayed on the case that faces the rotating blade. As the blade elongates, it will rub first on the abradable coating, which is designed to be easily rubbed, and serves as a sacrificial material. A wear scar in the shape of the blade tip will form on the coating. Consequently, the blade remains undamaged, clearance is maintained at the smallest scale, and engine efficiency is increased.

The lack of research has led to blade wear and transfer behavior, including coating transfer to the blade and vice versa, occurring frequently in the engine. This situation seriously threatens engine security and decreases engine efficiency.

Numerous studies on the high-speed rubbing behavior between a blade and an abradable seal coating have been conducted to address the aforementioned problem. Borel, et al. *(1)* drew a wear mechanism map of AlSi–plastic coating and Ni–graphite coating based on the correlations obtained between test values and wear mechanisms. Both blade wear and coating adhesion to the blade were seriously influenced by the test parameters. For example, AlSi–plastic coating with low-melting plastic (molten at 350°C) transferred to the blade during high-speed rubbing under most test conditions at extremely high linear speeds (≥400 m/s). The blade was then melted by high frictional heat, thereby resulting in blade wear. Bill and Shiembob *(2)* studied the wear behavior of three types of seal coatings under a range of working conditions and predicted that a low incursion rate tended to promote smearing, with consequent wear to the knife edge. Stringer and Marshall *(3)* found that a single pass depth exerted considerably great influence on the wear mechanism, with tests at a high single-pass depth showing minimal wear or adhesion, whereas tests at a low single-pass depth showed significant adhesion and wear. Fois, et al. *(4)* used a stroboscopic imaging technique to identify three phases for adhesive transfer during a test: (1) an initiation phase with a low adhesion rate, (2) a steady-state adhesion phase, and (3) the fracture of the adhered material followed by reinitiation. However, both Stringer and Marshall *(3)* and Fois, et al. *(4)* gave minimal attention to the mechanism of coating adhesion to the blade. Laverty *(5)* conducted a rub energy study and reported that the incursion rate exerted the greatest influence, in which coating transfer to blade and blade wear were aggravated at a high incursion rate. Bounazef, et al. *(6)* studied the transfer behavior of BN-SiAl-bounding organic element coating and found that coating transfer to the blade was minimal at a high linear speed and incursion rate but severe at a low linear speed and incursion rate.

In summary, most of the studies on high-speed rubbing between a seal coating and blade have focused on the relationship between test conditions and blade wear or transfer behavior. As to the more important issue, which is the mechanism of blade wear and material transfer, there is still no consensus explanation and few studies have been carried out on the issue. However, it is recognized that the high frictional heat due to a high sliding speed is the key impact factor on blade wear and

CONTACT Deli Duan duandl@imr.ac.cn

Color versions of one or more of the figures in the article can be found online at www.tandfonline.com/utrb.

Review led by A. Segall.

material transfer (Stringer and Marshall *(3)*; Kennedy *(7)*; Kennedy and Ling *(8)*). Yet, there are few research studies on the effects of frictional heat such as temperature rise and its relationship with thermal properties of rub pair materials. Obviously, these results have important impacts on the wear behaviors.

The current research includes a high-speed rubbing test of two types of abradable seal coatings. It attempts to discuss the mechanism of blade wear and transfer behavior from the perspective of temperature increase caused by frictional heat and by comparing the different wear behaviors of the two coatings. This research is significant to understand friction and wear behavior during high-speed rubbing. It is also helpful to engineering applications of seal coating.

Materials and methods

Materials

The blade sample for the rubbing test was cut from annealed Ti6Al4 V alloy via wire electrode cutting. The rubbed face of the blade sample was a 4 mm × 4 mm square. Before the test, the rubbed face of the blade sample was abraded with sandpaper to achieve a final surface roughness R_a of 0.5 μm, which is the average blade roughness in a real engine (ground by high-speed grinding). The blade sample was cleaned with absolute ethanol, dried in warm air, and preserved in a dryer.

Two different abradable seal coatings were tested for comparison. The first was Al-hBN, which is an Al-based seal coating, and the second was NiAl-hBN, an Ni-based seal coating. The most significant difference between the two coatings was their varied metal substrates. The other aspects, such as the spray method, solid lubrication phase, and transitional layer, were the same.

Both coatings sprayed using air plasma were developed for use in a compressor. The nominal constituents and weight percentage of the sprayed power for the NiAl-hBN coating were 67 wt% Ni, 8 wt% NiAl, and 25 wt% BN. For the Al-hBN coating, they were 75 wt% Al, 20 wt% BN, and 5 wt% Na_2SiO_3 binder. The spray parameters for Al-hBN coating are indicated in Table 1. For military secrecy, the spray parameters of NiAl-hBN coating cannot be given. Both substrates, which were made of stainless steel, were grit blasted before spraying. The metal-phase Ni (with about 8 wt% NiAl alloy) for the NiAl-hBN coating and Al for the Al-hBN coating served as the matrix and provided strength to the coating. The hBN was a solid lubricant that could decrease friction and mitigate wear. Both coatings had numerous porosities, which could promote its breakage during rubbing. To enhance bonding strength between the coating and the substrate, an NiAl transitional layer with a thickness of about 0.05 mm was first sprayed onto the substrate of both coatings. The spray parameters for NiAl layer are included in Table 1. The final thicknesses of the coatings were approximately 2 mm. The surfaces of the coating samples were first ground flat using a grinding machine and then abraded with sandpaper until an R_a of approximately 6 μm was attained. The roughness was determined based on estimation of the applied coating in the engine; the final coating surface was acquired through rough turning in a real engine.

Table 1. Spray parameters for Al-hBN coating and NiAl transitional layer.

Spray parameters	Unit NiAl transition layer	Al-hBN coating
Spray distance	140 mm	110 mm
Plasma gas (Ar) flow rate	90 L min^{-1}	90 L min^{-1}
H_2 flow rate	10 L min^{-1}	5 L min^{-1}
Arc current	550 A	400 A
Voltage	60 V	52 V
Powder feed rate	40 g/min	50 g/min
Carrier gas (N_2) flow rate	4 L min^{-1}	4 L min^{-1}

The hardness of all of the coating samples was tested on a surface Rockwell hardness tester (WRHS-60D, Beijing Wowei Science and Technology Company). The selected scale was HR15Y, which meant that the indenter was a half-inch ball, the load was 15 kg, and the dwelling time was 10 s. Only the samples with an HR15Y hardness value of approximately 50 were used. The section morphologies of the Al-hBN and NiAl-hBN coating are shown in Fig. 1.

Methods

All high-speed rubbing tests were conducted on a test rig built by our research group (Xue, et al. *(9)*). A sketch of the test rig is shown in Fig. 2. The blade sample is inserted into a metal disc driven by a high-speed motorized spindle and rotates quickly. The coating sample is fastened onto a sliding table and moves to the rotating blade at a given incursion speed and depth. As soon as the moving coating comes into contact with the rotating blade, the rubbing begins. The test parameters listed in Table 2 were selected based on the different flying stages of the engine. *Single-pass depth* refers to the incursion depth during a single rub in one blade rotation. *Incursion speed* refers to the sliding speed of the coating to the rotating blade.

The height change of the blade was recorded using a screw-thread micrometer with a precision of 1 μm. The macromorphologies of the blade and the wear scar of the coating were inspected using a digital camera. The micromorphologies were observed using a scanning electron microscope (SEM). The element distribution on the surface of the wear scar was studied with an energy-dispersive spectrometer (EDS). The thermal conductivity of the coating was determined using an unsteady heat conduction method on a thermal property analyzer. The thermal diffusivity of the coating was acquired through a laser pulsing method. The process included testing each coating three times in a chamber at temperatures ranging from 200 to 300°C. The average of six tests was the value used in the study. The density of the coating was determined using a weighting method. The melting point of the coating was determined via differential thermal analysis (DTA). Due to the different thermal limits of the two coatings (the metal matrix Ni of NiAl-hBN coating has a higher melting point than the metal matrix Al in the Al-hBN coating), different test processes were employed to determine the coating melting

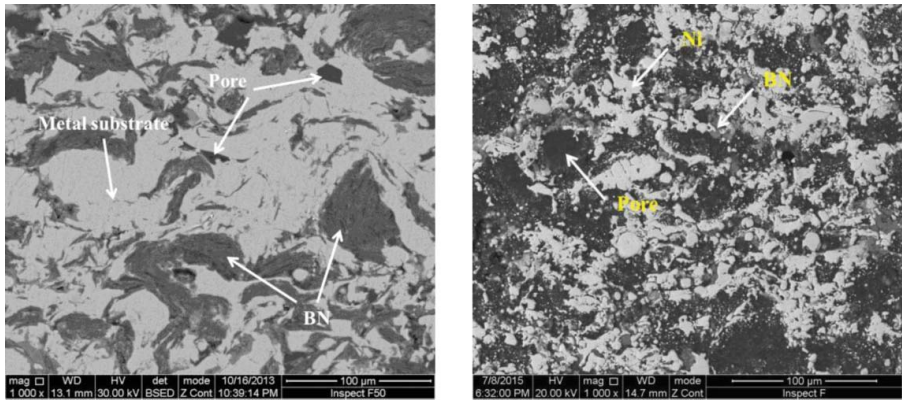

Figure 1. Section morphologies of the Al-hBN and NiAl-hBN coating: (a) Al-hBN coating and (b) NiAl-hBN coating.

point. The testing process for the Al-hBN coating was as follows. First, the coating was rapidly heated to 200°C and maintained at this temperature for 5 min. Then, the coating was heated to 700°C at a heating rate of 10°C/min and finally rapidly cooled to room temperature. The testing process for the NiAl-hBN coating began by rapidly heating the coating to 500°C and then maintaining it for 5 min at this temperature. Then, the coating was heated to 1500°C at a speed of 10°C/min and finally rapidly cooled to room temperature.

Results

Blade height variation results

The blade height variations after rubbing with the two coatings at varying single-pass depths and linear speeds are shown in Fig. 3. All of the values were calculated by subtracting the pretest value from the posttest value, which means that a negative value indicates the height loss and a positive value indicates the height gain. As shown in the figure, the heights of the blades that rubbed against the NiAl-hBN coating decreased under all test conditions, whereas the heights of the blades that rubbed against the Al-hBN coating increased. Posttest observations showed that the coating materials adhered to the blades rubbed against the Al-hBN coating, and the height increase was believed to be the result of such adhesion. In addition, the height decrease of the blades rubbed against the NiAl-hBN coating was attributed to blade wear.

With regard to the influence of the test parameters, the adhesion of the Al-hBN coating to the blade was highest when the single-pass depth was low and the linear speed was high. The wear of the blade rubbed against the NiAl-hBN coating increased with linear speed when the single-pass depth was constant.

Rubbed by the blade of same material, the two coatings displayed completely different wear behaviors, which were believed to be relative to the different coating thermophysical properties.

Material transfer behavior of the Al-hBN coating

As shown in Fig. 3, blade height increased significantly during the tests at a low single-pass depth, and linear speed profoundly affected blade height. Hence, blade and coating wear scars rubbed at the lowest single-pass depth of 0.085 μm and two linear speeds (30 and 150 m/s) were checked.

Figure 4a shows that the coating material adheres to the rubbed blade. An increase in blade height resulted from such adhesion, which was not uniform. Two separate regions of the blade tip were covered by the coating

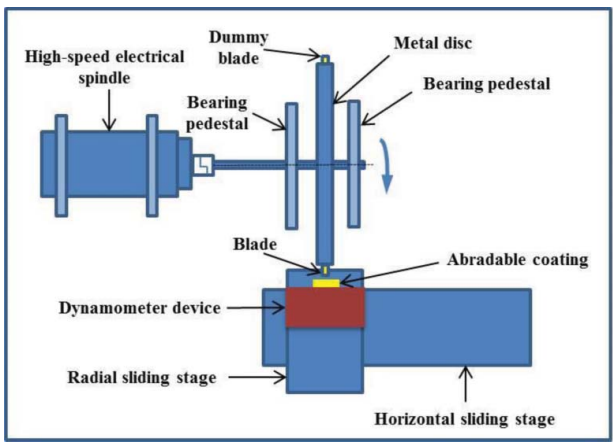

Figure 2. Sketch of the high-speed test rig.

Table 2. Test parameters used in the study.

Single-pass depth (μm)	Linear speed (m/s)	Incursion speed (μm/s)	Incursion depth (μm)
0.085	30	2	400
0.085	90	6	400
0.085	150	10	400
0.142	30	3	400
0.142	90	9	400
0.142	150	15	400
0.856	30	20	400
0.856	90	60	400
0.856	150	100	400
4.264	30	100	400
4.264	90	300	400
4.264	150	500	400
7.107	30	167	400
7.107	90	500	400
7.107	150	833	400

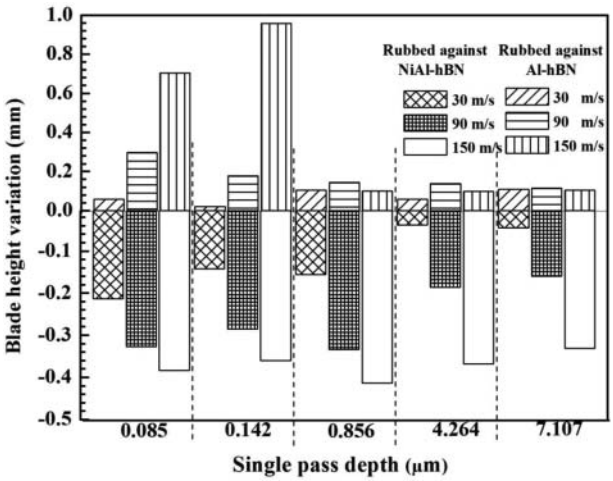

Figure 3. Blade height variations after rubbing with the two coatings at different linear speeds and single-pass depths.

material, whereas the remaining area was nearly bare. As shown in Fig. 4b, coating material adhesions on the blade were lamellar and scattered on the blade tip. As can be seen form Fig. 4c, the coating wear scar was divided into two separated grooves that corresponded to the two adhered regions on the blade. Plastic deformation and smearing are observed in Fig. 4d, whereas the remaining area displayed spalling. The smeared area corresponds to the shiny metal-colored area in the wear scar in Fig. 4c. EDS analysis was conducted on the smeared and spalling region of the wear scar. The spectrum and element atomic percentage are shown in Fig. 5. Metal Al was the main composition in region 1 and no B was detected, which indicated that the metal-phase Al in the coating wear scar was smeared and the shiny metal color belonged to metal Al. A comparison of Figs. 4a and 4c showed that the adhesion on the blade tip displayed a shiny metal color that indicated that the smeared metal Al transferred to the blade tip. In region 2, which represented coating spalling, the main composition was B from the solid lubrication, which accounted for nearly 50%. Hence, coating spalling occurred when a large amount of solid lubrication BN was present.

The blade and coating wear scar morphologies rubbed at 150 m/s and 0.085 μm are shown in Fig. 6. The blade profile in Fig. 6a indicates that the adhesion formed a thick layer that covered the blade tip. This result is in accordance with the measured height variation. The SEM image

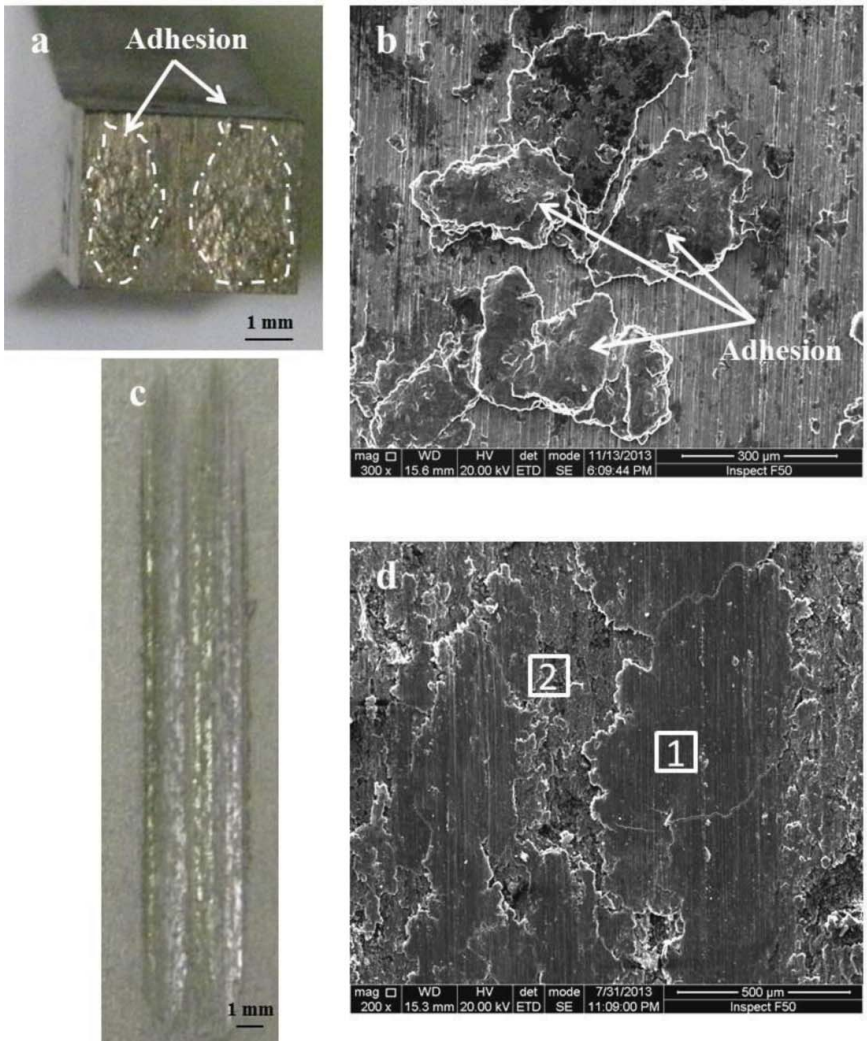

Figure 4. Macromorphology and SEM picture of (a), (b) blade and (c), (d) Al-hBN coating wear scars tested at 30 m/s and 0.085 μm.

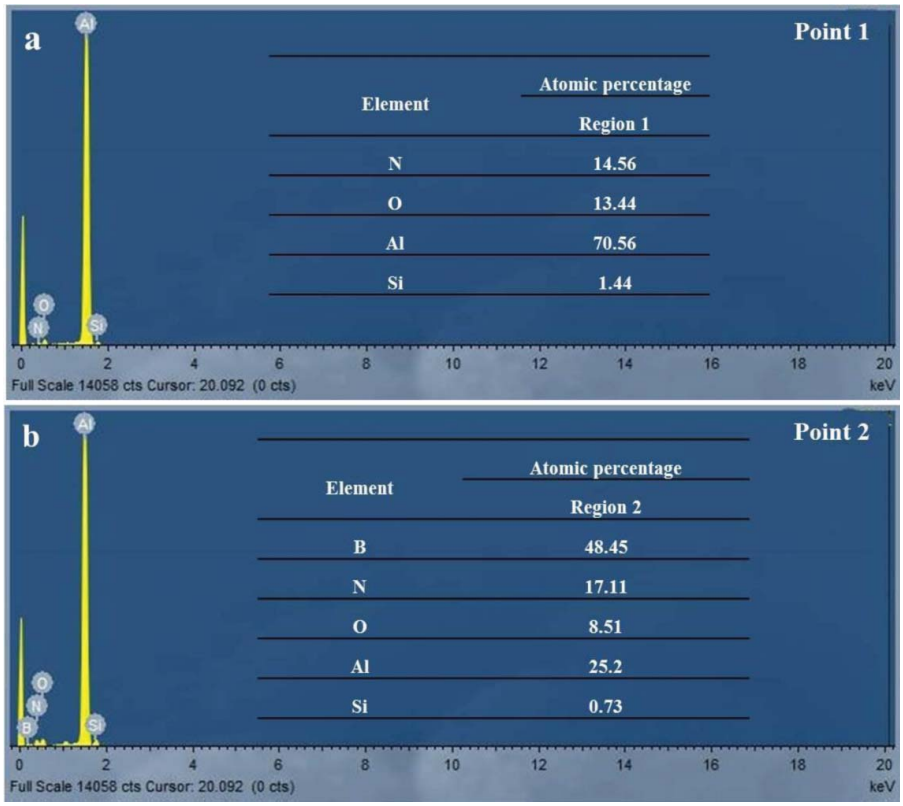

Figure 5. EDS spectrum and element atomic percentage of regions 1 and 2 in Fig. 4d.

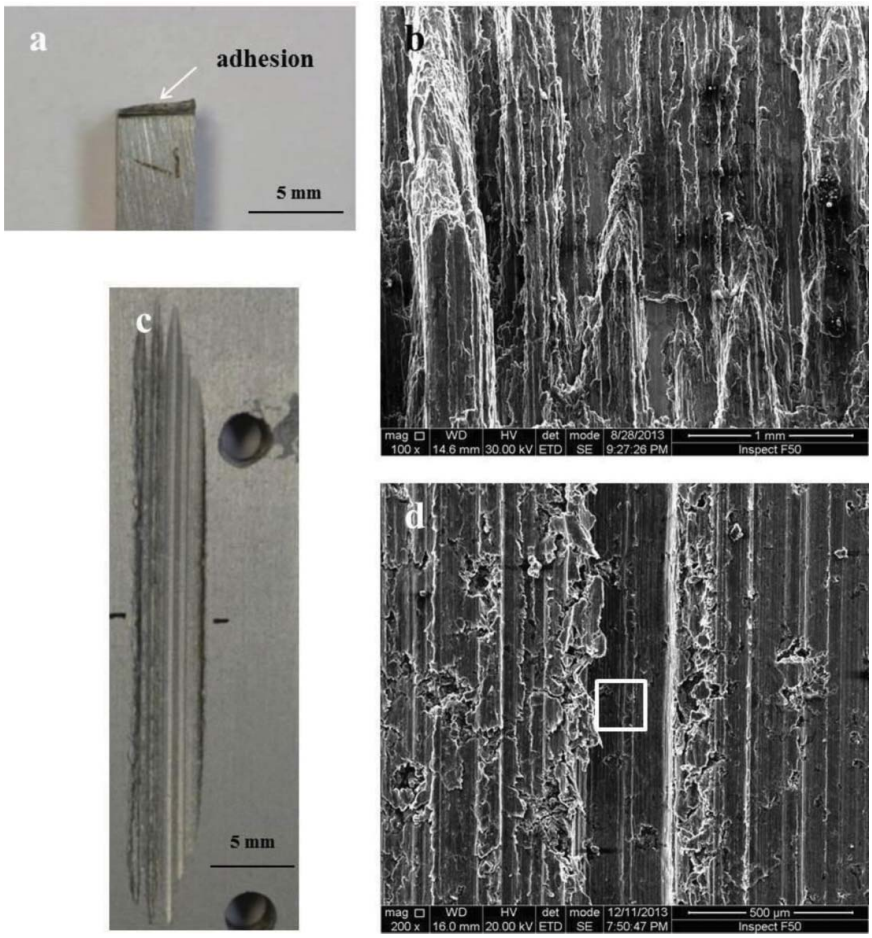

Figure 6. Macromorphology and SEM picture of (a), (b) blade and (c), (d) Al-hBN coating wear scars tested at 150 m/s and 0.085 μm.

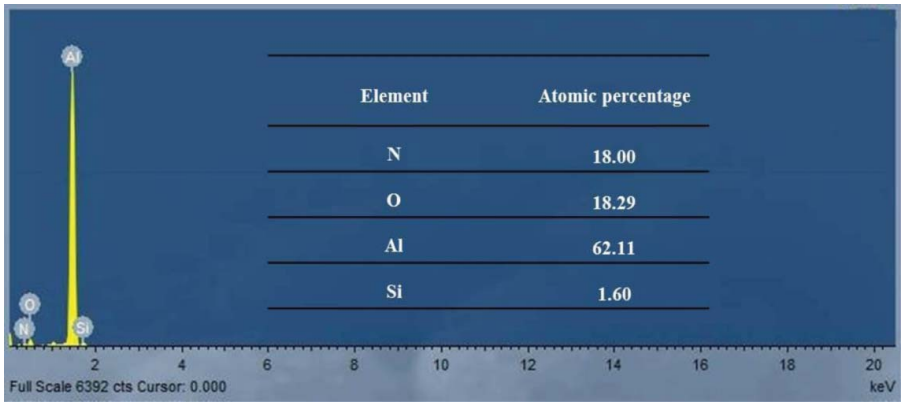

Element	Atomic percentage
N	18.00
O	18.29
Al	62.11
Si	1.60

Figure 7. EDS spectrum and element atomic percentage of the rectangular area in Fig. 6d.

(Fig. 6b) showed that the coating material was smeared on the blade tip and formed a dense layer that was significantly different from the scattered layer of 30 m/s. As shown in Fig. 6c, many furrows that emerged in the coating wear scar corresponded to the uneven adhesion on the blade. Microrupture and ploughing were the main coating wear mechanisms, as shown in Fig. 6d. The EDS spectrum and test results of the rectangular area in Fig. 6d are presented in Fig. 7. Compared with the results in Fig. 5, the main composition was metal Al and no B was detected.

The preceding results indicated that the B element disappeared in the coating wear scar when coating adhesion occurred. As is known, BN functions as a solid lubrication that can decrease coating adhesion to the blade. Coating adhesion was believed to be related to the missing BN during rubbing.

Material transfer behavior of the NiAl-hBN coating

Compared with the Al-hBN coating, the high-speed wear behavior of the NiAl-hBN coating rubbed by the same Ti6Al4 V blade was completely different, although only the metal phase was changed.

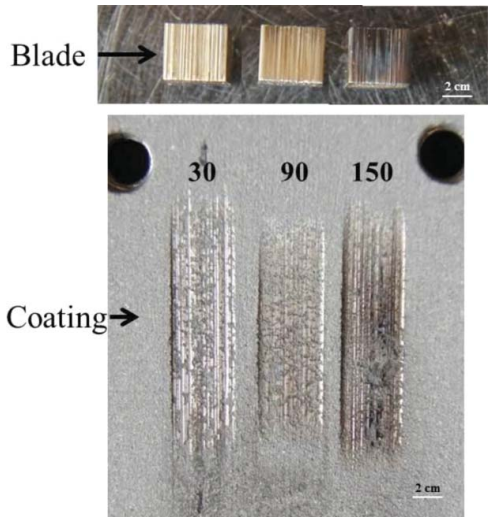

Figure 8. Wear scar morphologies of the rubbed blade and NiAl-hBN coating tested at the lowest single-pass depth and different linear speeds.

To compare with the Al-hBN coating, the wear scar morphologies of the rubbed blade and the coating tested at the lowest single-pass depth and different linear speeds are presented in Fig. 8. No adhesion was found on the blade tip. The colors of the blade tip were different after rubbing at different linear speeds. The oxidation study of the Ti alloy indicated that the oxide color changed from silvery white to light yellow to deep yellow to deep blue to grayish blue with increasing furnace temperature (Luo, et al. *(10)*). Different colors were produced by varying oxidation levels, which resulted in various Ti oxides. For the tests conducted in this study, oxidation of the blade tips became more severe at higher linear speeds. The intense frictional heat due to a high linear speed was believed to be responsible for the oxidation.

As shown in Fig. 8, many fragments with a metal shine are scattered on the coating wear scar. Compared with the blade, the fragments had the same color as the rubbed blade tip. Hence, the fragments could have come from the transfer of the blade material to the coating during rubbing.

SEM pictures of the blade wear scars are shown in Fig. 9. No adhesion could be found on the blade tips. Furrows and plastic smearing were observed after rubbing at 30 m/s. At 90 m/s, a large area of plastic flow appeared on the blade tip. At 150 m/s, a layer full of cracks nearly covered the blade tip. This layer was believed to be an oxidation film.

Blade oxidation was aggravated at a higher linear speed as indicated by the color change of the rubbed blade tip. The SEM picture (Fig. 9c) also presented a layer that was recognized as an oxidation film. To further validate this conclusion, a minor angle and parallel light XRD test was conducted on the rubbed blade tips. The peak identification obtained by universal XRD peak search and matching software is presented in Fig. 10. Peaks that belonged to TiO were detected, which indicated that oxidation occurred during the rubbing performed at different linear speeds. At 30 m/s, the main peak (located at 44°) of TiO was extremely low. As the linear speed increased, the main peak intensity became higher, which proved that blade oxidation intensified at high linear speeds.

The micromorphologies of the coating wear scars are shown in Fig. 11. Many fragments full of cracks adhered to the wear scar surface in accordance with the macromorphology

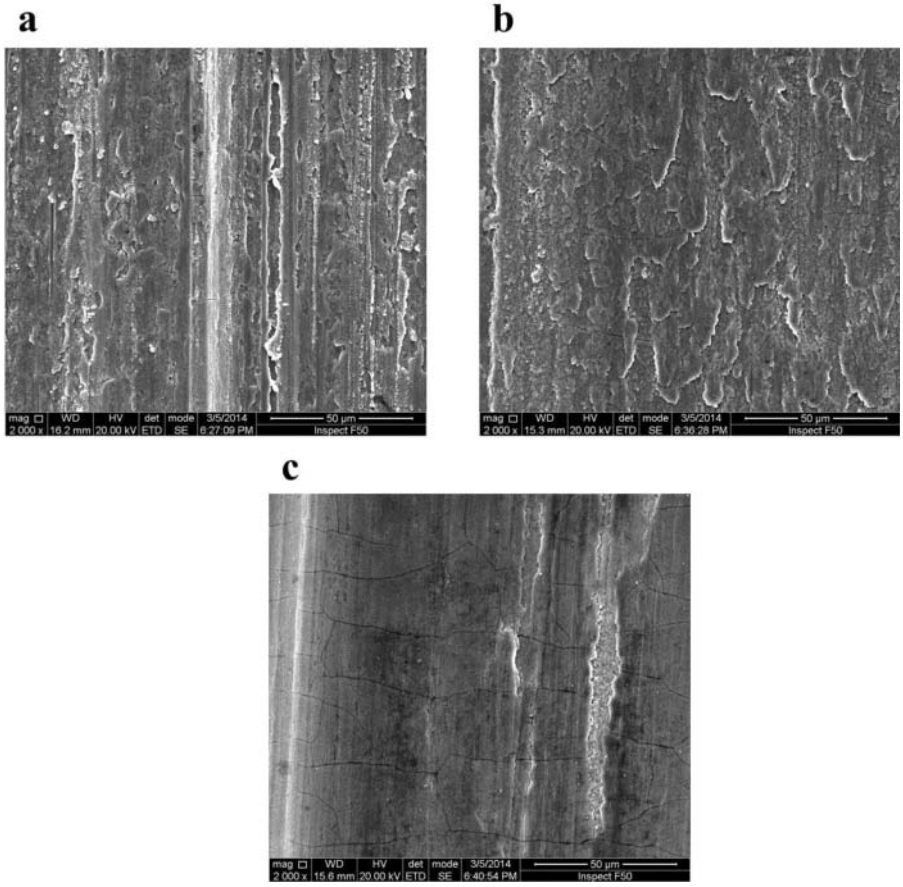

Figure 9. Surface morphologies of the blade rubbed against NiAl-hBN coating tested at (a) 30 m/s, (b) 90 m/s, and (c) 150 m/s when the single-pass depth was 0.085 μm.

observation (Fig. 8). The remaining area without covered fragments exhibited a spalling morphology. EDS detection was conducted to identity the composition of the fragments. The results are presented in Fig. 12.

The main composition included Ti and O, and coating material Ni was also detected. This observation indicated that the fragments resulted from blade material that was transferred and mixed with the coating material. A transfer/mixed layer was formed on the coating wear scar. In addition, the ratio of O and Ti increased with linear speed, thereby proving once more the previous conclusion regarding blade oxidation. In summary, blade oxidation wear occurred and blade material transferred to the NiAl-hBN coating with the formation of a transfer/mixed layer during high-speed rubbing.

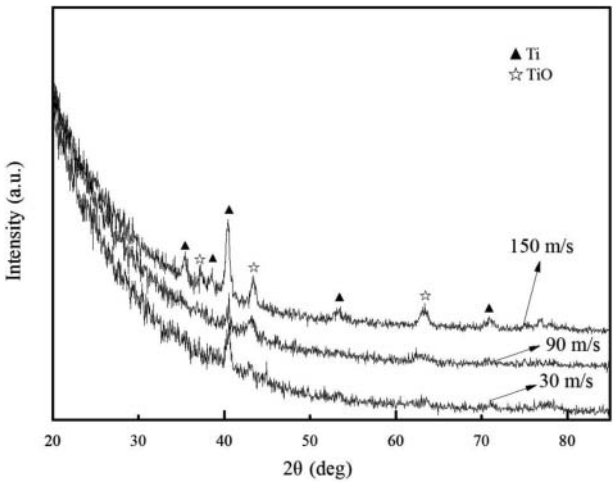

Figure 10. XRD test results of the blade tips rubbed against NiAl-hBN coating at different linear speeds with the single-pass depth maintained at 0.085 μm.

Discussion

Comparison of the transfer mechanisms of the two coatings

The tests of the Al-hBN and NiAl-hBN coatings rubbed by the same Ti6Al4 V blade indicated that Al-hBN coating material transferred to the blade, whereas blade material transferred to the NiAl-hBN coating during rubbing. Both transfers significantly influence the abradability of the rubbing system. In addition to transfer direction, the structure and composition of the resulting transfer layer were compared.

As shown in Fig. 13, the transfer layer of the Al-hBN coating to the blade tip has a layered structure. Evident gaps were observed on the blade side, which indicated that blade wear occurred simultaneously. The result of EDS detection showed that the main composition was coating material Al, and a trace of blade material Ti was found. Metal Al in the transfer layer exhibited a short, thin strip form that was different from the

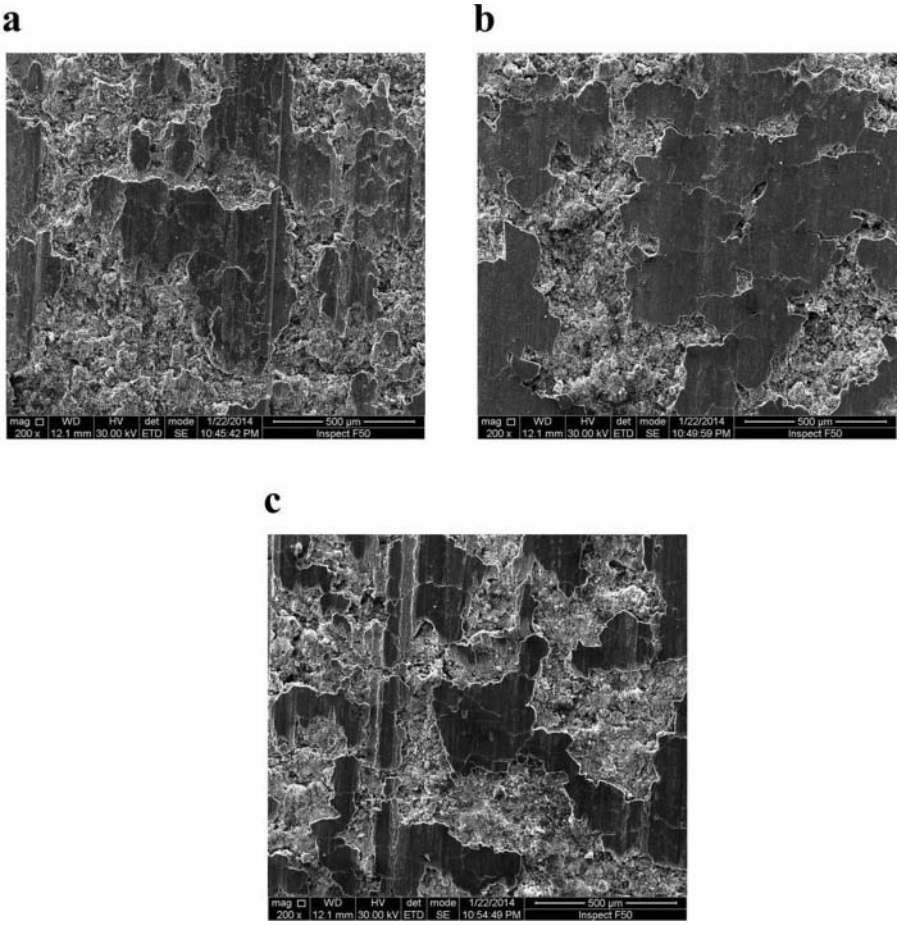

Figure 11. Surface morphologies of the NiAl-hBN coating wear scars at different linear speeds of (a) 30, (b) 90, and (c) 150 m/s for a constant single-pass depth of 0.085 μm.

large flake shape in the unrubbed coating. BN could not be found in either the morphology observation or the EDS detection. In relation to the observed smeared metal Al in the coating wear scar (Figs. 4c, 4d, 6c, 6d), transfer resulted from the accumulation of deformed and melted metal-phase Al. This process was assisted by burning (oxidation) of the lubrication-phase BN. Both behaviors were attributed to the intense frictional heat generated during high-speed rubbing. Before metal-phase Al was softened, blade wear occurred in the form of abrasive wear, and wear debris was included in the transfer layer. Hence, a trace of Ti was detected.

The SEM micromorphology of the transfer/mixed layer surface in the NiAl-hBN coating wear scar rubbed at 0.085 μm and 90 m/s is shown in Fig. 14. The rubbing direction is indicated by an arrow. Tadpole-like adhesions appeared. The adhesion had a round head with longer or shorter tails dragging behind. The direction of drag was in accordance with the rubbing direction.

EDS detection was conducted to determine the composition of the tadpole-like adhesion. The results are presented in Fig. 15. The main components O and Ti were found in both the head and the tail of the tadpole-like adhesion. In addition, the atomic percentages of O and Ti in the two regions were close. Considering the shape of the tadpole-like adhesion, the blade tip experienced plastic flow caused by the intense frictional heat generated during high-speed rubbing. In addition, the softened blade tip was sheared and smeared on the coating wear scar. The agreement between the adhesion tail drag direction and rubbing direction reflected the aforementioned assumptions.

The SEM micromorphology of the transfer/mixed layer surface in the NiAl-hBN coating wear scar rubbed at 0.856 μm and 150 m/s is shown in Fig. 16. A distinct layered smear adhered to the surface of the transfer/mixed layer. The smear had a strip shape, which was wide at the top and narrow at the bottom. The top smear did not completely cover the bottom transfer/mixed layer. The formation mechanism of the strip smear was assumed to be same as the tadpole-like adhesion. Both resulted from the shearing and smearing of the softened blade tip. The different appearance of the strip smear was attributed to the subsequent rubbing of the tadpole-like adhesion. More or less rubbing occurred after the test was stopped because the withdrawal speed of the coating was relatively low compared with the rotating speed of the blade. These rubs changed the tadpole-like adhesion into strip smears. The rare tadpole-like adhesion was preserved because rubbing occurred when no further contact occurred between the blade and the coating after shearing of the softened blade tip during the last rubbing.

The section micromorphology of the coating wear scar resulting from the rubbing at 0.142 μm and 150 m/s is shown in Fig. 17. The thickness of the transfer/mixed layer was observed to be approximately 20 μm. Upon careful examination, the transfer/mixed layer was found to be layered and full

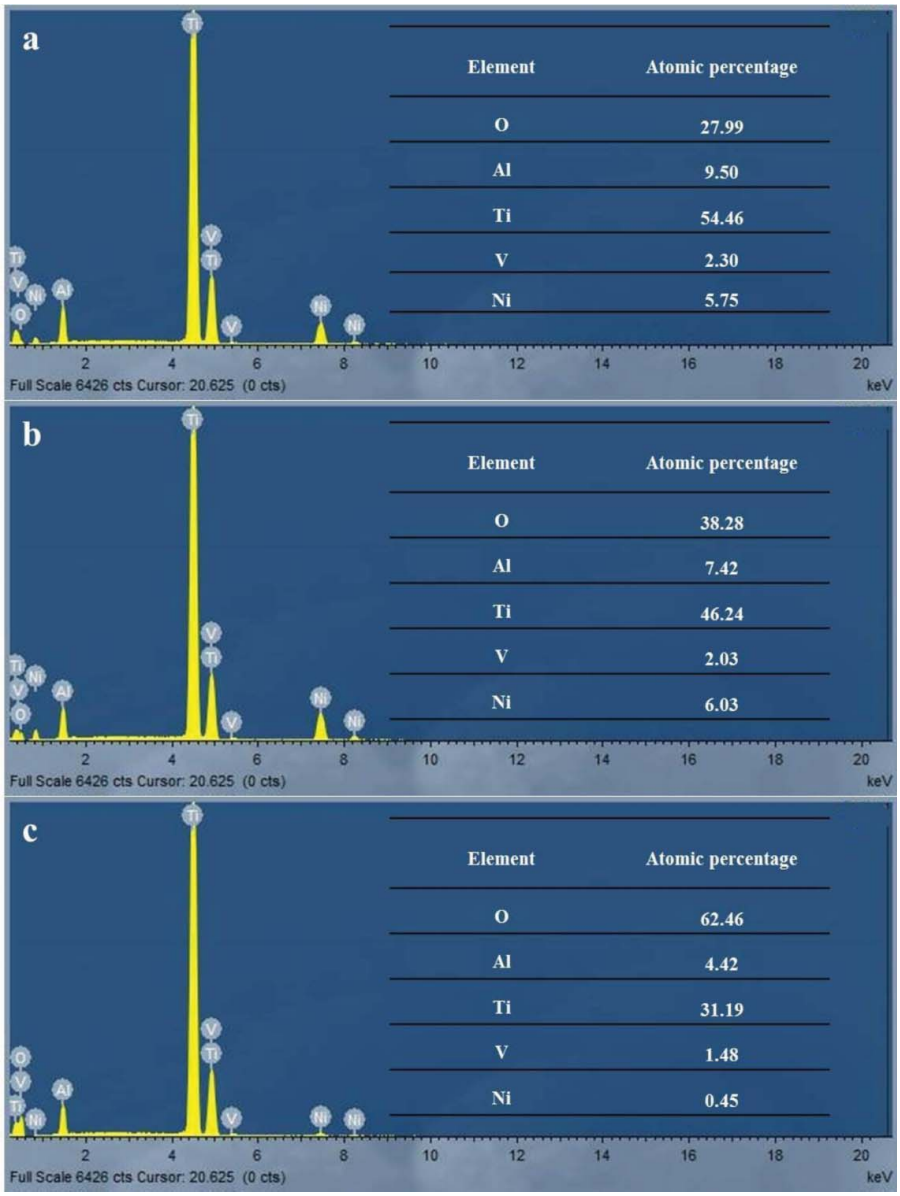

Figure 12. EDS spectrum and element atomic percentage of the fragments in NiAl-hBN coating wear scars (Fig. 11): (a) 30 m/s, (b) 90 m/s, and (c) 150 m/s.

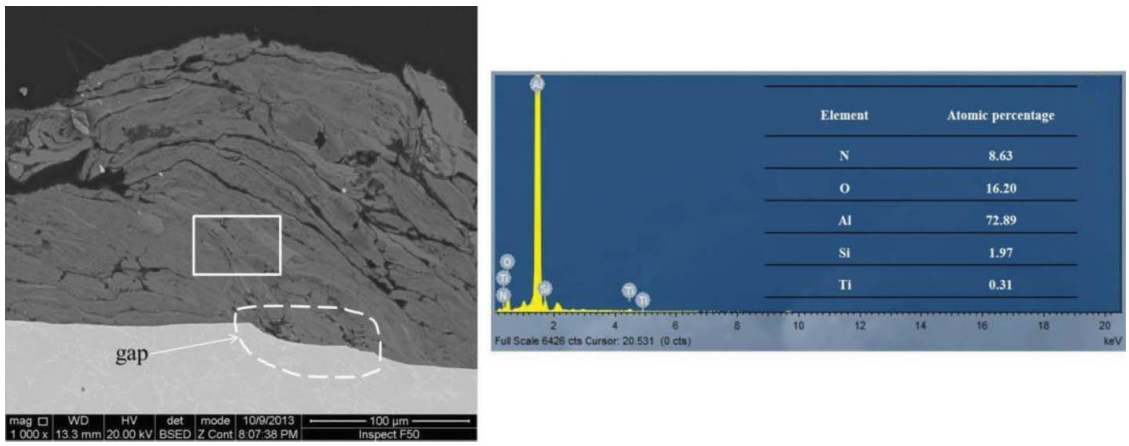

Figure 13. Micromorphology and EDS detection results of the transfer layer section on the Ti6Al4 V blade tip rubbed against Al-hBN coating at 90 m/s and 0.085 μm.

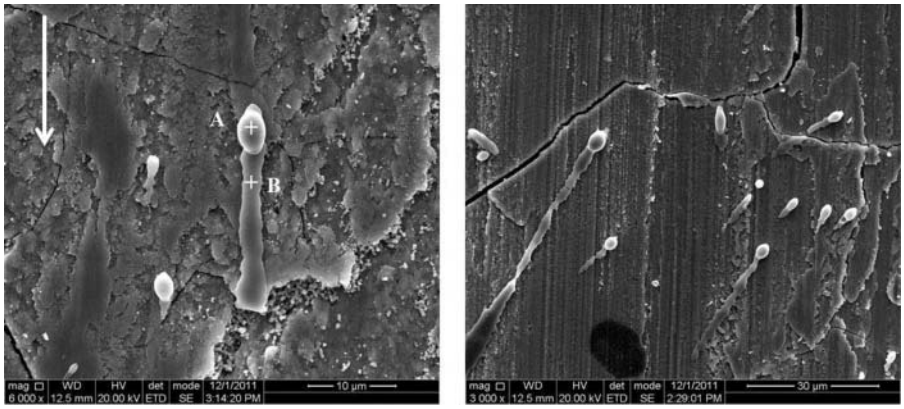

Figure 14. SEM picture of the transfer/mixed layer in the NiAl-hBN coating wear scar rubbed at 90 m/s when the single-pass depth was 0.856 μm.

of cracks. At the top of the transfer/mixed layer, an extremely thin layer, which had a clear boundary with the bottom layer, adhered. This finding proved that the transfer/mixed layer was produced by successive smearing of the softened blade tip.

In summary, Al-hBN and NiAl-hBN coatings exhibited different transfer directions when rubbed using the same Ti6Al4 V blade. Al-hBN coating material transferred to the blade and formed a layered transfer layer on the blade tip. Blade material transferred to NiAl-hBN coating and resulted in a transfer/mixed layer, which was lamellar in the coating wear scar. Both the transfer layers were lamellar, which indicated that both effects were produced by successive rubbing. For the Al-hBN coating, deformed and melted metal Al were continuously smeared on the blade tip during rubbing. Conversely, softened and melted blade material transferred to the coating wear scar when rubbed against the NiAl-hBN coating. Blade material transferred to the coating easily mixed with the coating material because of the relative motion setting, in which the rotating blade incurred stationary coating. For the Al-hBN coating, the transfer layer on the blade tip had nearly no blade material, although blade wear occurred.

The two coatings presented varied wear behaviors. The different temperatures reached as generated by the rubbing could have led to considerable differences.

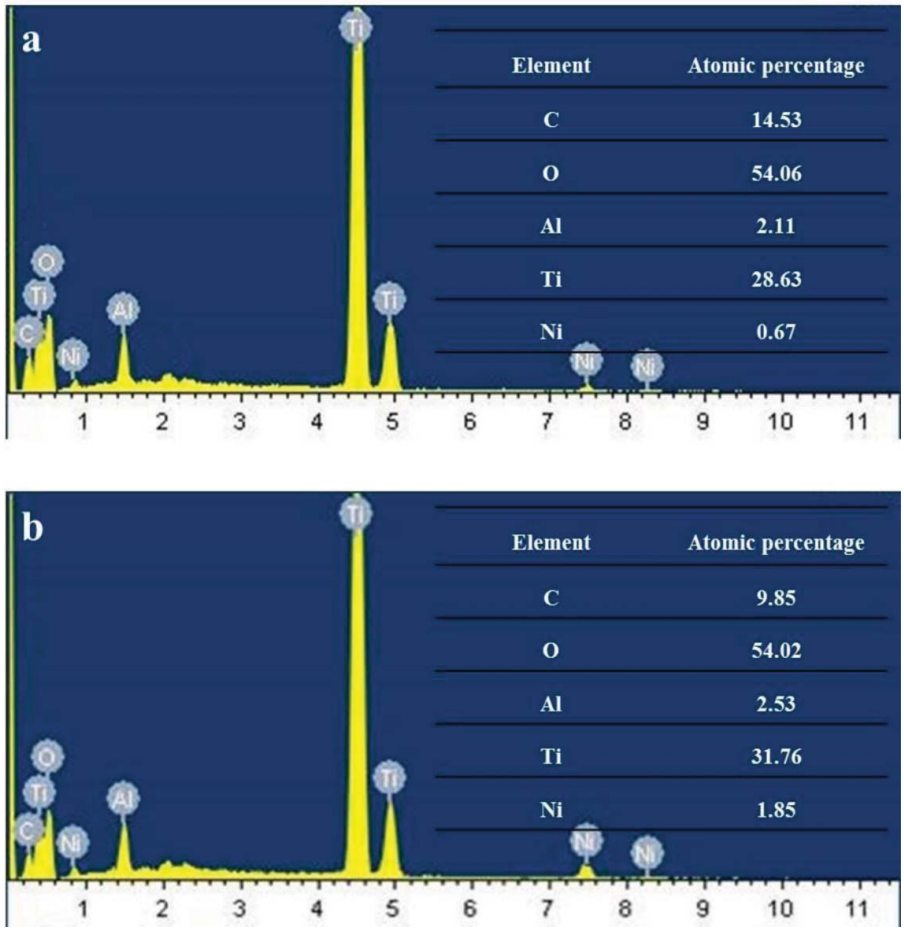

Figure 15. EDS detection results of the points (a) A and (b) B in Fig. 14.

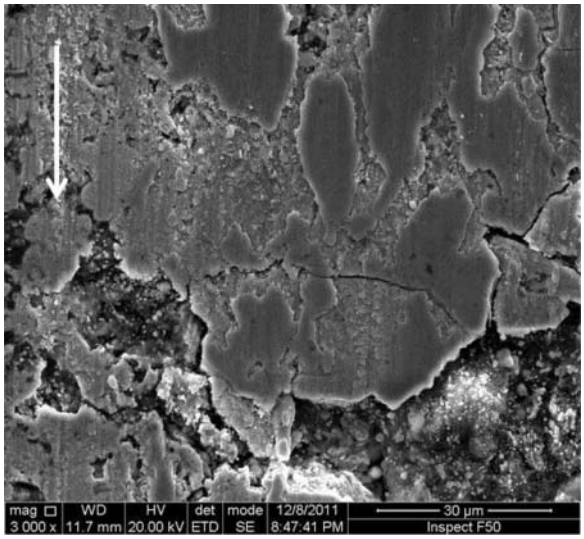

Figure 16. SEM micromorphology of the transfer/mixed layer surface in the NiAl-hBN coating wear scar rubbed at 0.856 μm and 150 m/s.

Influence of frictional heat

During the friction and wear process, nearly all energy dissipated by friction appeared as heat, and heat was removed from the contact surface via conduction and radiation Rigney and Hirth *(11)*; Uetz and Föhl *(12)*; Bowden and Tabor *(13)*). The generation and dissipation of the frictional heat occurred in the contact area between asperities given that the true contact areas between the friction pair are asperities. The highest temperatures, which occurred close to the asperities, were of short duration and sometimes called flash temperatures (Archard *(14)*; Blok *(15)*). A high flash temperature indicates severe friction or wear, particularly when the sliding speed is high. This value is significant for understanding friction and wear behavior; for example, determining whether the flash temperature reaches the phase transition temperature of the contact materials or is sufficiently high to melt one of the contact materials. However, measuring the flash temperature directly is nearly impossible because of its short duration and the small areas between

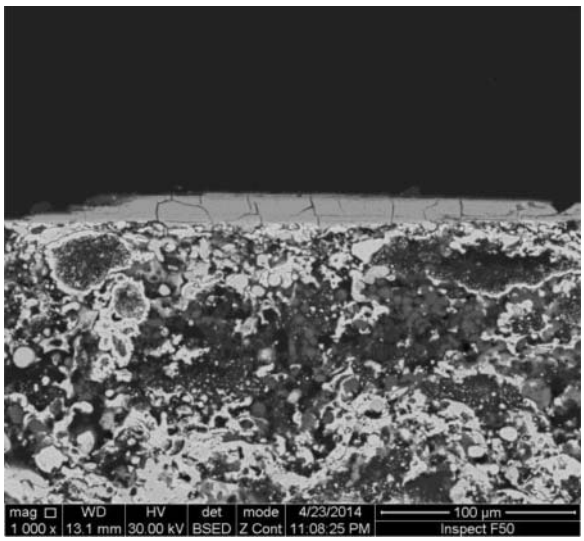

Figure 17. Section micromorphology of the NiAl-hBN coating wear scar resulting from rubbing at 0.142 μm and 150 m/s.

Table 3. Parameters used in calculating the rubbing interface temperature.

Coatings	a (m)	V_B (m/s)	χ_C ($10^{-6}m^2s^{-1}$)	K_C ($Wm^{-1}K^{-1}$)	L
Al-hBN	0.002	150	12	23	1.3×10^4
NiAl-hBN	0.002	150	6	10	2.5×10^4

contacting asperities. Accordingly, theoretical analysis was adopted to study flash temperature.

According to the theoretical analysis introduced in the Appendix, in this study, the rotating blade sample could be regarded as body B (Fig. A1) and the coating sample as body C (Fig. A1). To estimate the temperature of the contact area between the blade and the coating sample, we should firstly determine the dimensionless quantity L in the Appendix of the two coatings. For testing, we used the rubbing speed of 150 m/s as an example. The thermal diffusivity and conductivity of the coating were obtained using thermal analysis equipment. The actual contact area was a square with a side measuring 0.004 m and was replaced simply by a circle with a radius of 0.002 m in the calculation. From Eq. [A3] in the Appendix, the calculated L of the two coatings is shown in Table 3. The L values of both Al-hBN and NiAl-hBN were higher than 5. When L_C in Eq. [A8] of the Appendix was replaced with the calculated L, and L_B of the blade sample was 0, $\zeta \to 1$, which indicated that a large fraction of frictional heat passed to the coating sample. Consequently, the surface temperature of the contact area was mainly determined by the thermophysical properties of the coating, and the calculation formula of Eq. [A5] in the Appendix should be used.

As indicated in Eq. [A5] in the Appendix, using the relationship $\chi = K/\rho C$, it can be found that the higher the coating thermal conductivity or the coating diffusivity, the lower the contact surface temperature. This result was proven via the thermomechanical simulation of the high-speed rubbing of a seal coating performed by Kennedy *(7)*. Moreover, the experimental study on sliding metals conducted by Bowden and Tabor *(13)* showed that surface temperature increased with a decrease in the thermal conductivities of the contacting metals.

For the tests conducted in this study, the application of Eq. [A5] in the Appendix indicated that the ratio of the surface temperatures of the two coatings rubbed by the same blade samples was

$$\frac{\theta_{\mathrm{NiAl-hBN}}}{\theta_{\mathrm{Al-hBN}}} = \frac{Q_{\mathrm{NiAl-hBN}}}{Q_{\mathrm{Al-hBN}}} * \frac{K_{\mathrm{Al-hBN}}}{K_{\mathrm{NiAl-hBN}}} * \left(\frac{\chi_{\mathrm{NiAl-hBN}}}{\chi_{\mathrm{Al-hBN}}}\right)^{\frac{1}{2}}. \quad [1]$$

Assuming that frictional heat generation was the same during the high-speed rubbing between the two coatings and the blade, we placed the corresponding values in Table 3 into Eq. [1] and obtained the following:

$$\theta_{\mathrm{NiAl-hBN}} \approx 1.6\theta_{\mathrm{Al-hBN}}. \quad [2]$$

As shown in Eq. [2], the attainable average temperature of the contact surface rubbed with the NiAl-hBN coating was 1.6 times that of the contact surface rubbed with the Al-hBN coating. The maximum temperature of the blade when rubbed

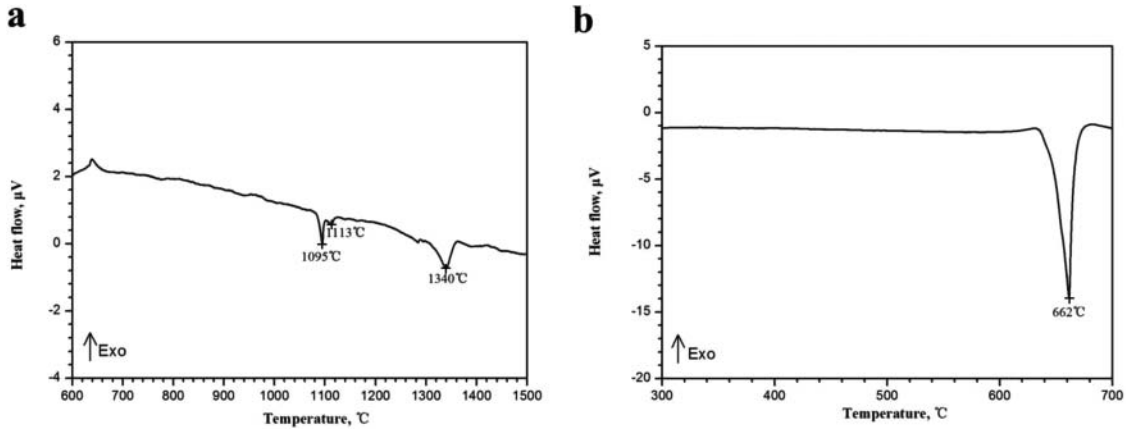

Figure 18. DTA curves of the two coatings: (a) NiAl-hBN and (b) Al-hBN.

with the NiCrAl coating was 1565 K, and it decreased to 865 K when rubbed with the AlSi coating, as predicted by the thermal model built by Wang *(16)*. The results obtained using the optical pyrometer agreed with those of the thermal model. The study by Wang *(16)* proved the correctness of Eq. [2] to a certain extent given the similarity of the studied coatings with the coatings used in the current study.

In addition to the thermal conductivity and diffusivity of the rubbed material, the attainable temperature of the contact area was related to the melting point of the rubbed material. The experiment performed by Bowden and Tabor *(13)* showed that having an interface temperature that was higher than the melting temperature of the rubbed material with a lower melting point in the friction pair during sliding was nearly impossible. The measured DTA curves of the two coatings are shown in Fig. 18. For the Al-hBN coating, an endothermic peak at 660°C indicated the melting of metal Al. For the NiAl-hBN coating, an endothermic peak emerged at 1340°C, which corresponded to the melting of metal Ni.

Related to the discussion on the transfer mechanism of the Al-hBN coating in Section Material transfer behavior of the Al-hBN coating, the metal-phase Al in the Al-hBN coating was melted during high-speed rubbing. The corresponding temperature was approximately 660°C, which was lower than the softening temperature of Ti6Al4 V. The melted Al transferred to the blade tip through rubbing. This process could have been promoted by the disappearance of the BN phase, which probably resulted from burning and spalling. Because the maximum flash temperature could be higher than 1000°C (indicated by many tests at even lower linear speeds; Chassaing et al. *(17)*, *(18)*; Rahaman and Zhang *(19)*; Tzanakis, et al. *(20)*) in the contact areas between asperities, burning of BN could occur. The wear debris collected during the high-speed test was checked. As shown in Fig. 19, debris containing metal Al and BN was found, which indicated that solid lubricant BN could peel off with metal Al.

The attainable temperature at the interface during rubbing with the NiAl-hBN coating was higher because of different thermal conductivities and diffusivities. This temperature was predicted to be approximately 1000°C by Eq. [2] considering that the temperature of the Al-hBN coating was of 660°C. Studies on similar coatings conducted by Emery, et al. *(21)* and Zenas, et al. *(22)* also reported a temperature higher than 1000°C. However, unlike that in the Al-hBN coating, the melting point of metal Ni in the NiAl-hBN coating was higher than 1000°C, and melting of the coating that could result in transfer did not occur.

Temperature significantly influences the mechanical properties of Ti alloy, and many studies have reported this phenomenon. Porntadawit, et al. *(23)* investigated the stress–strain

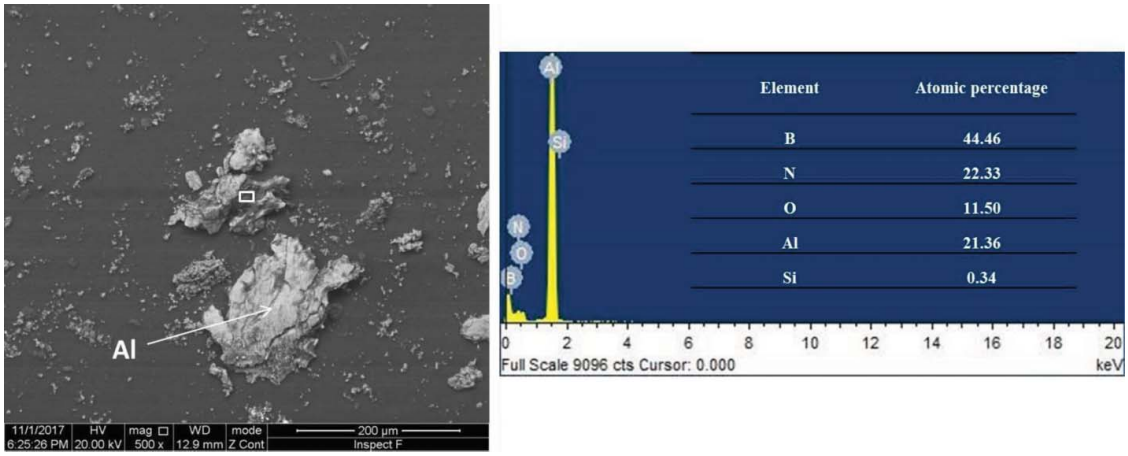

Figure 19. SEM picture of wear debris from Al-hBN coating and the EDS detection result of the rectangular area.

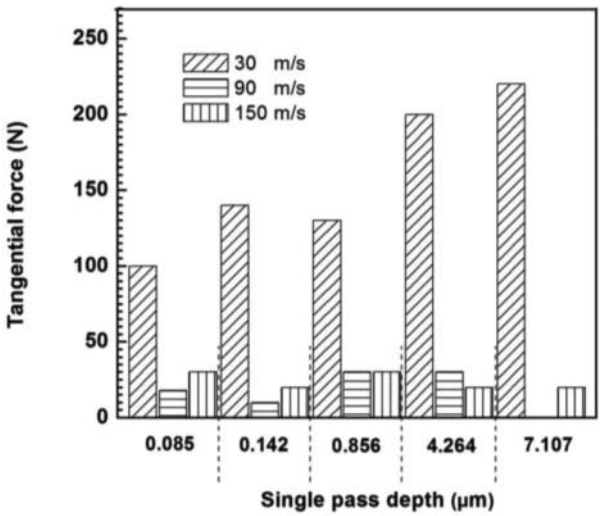

Figure 20. Tangential forces acquired during rubbing with the NiAl-hBN coating at different linear speeds and single-pass depths.

responses of Ti-6 Al-4 V alloy using compression tests at different elevated temperatures and strain rates. The Ti6Al4 V sample demonstrated plastic flow softening when the temperature reached 1000°C, and the corresponding flow stress did not exceed 100 mPa. Similar studies have found identical results (Ding, et al. *(24)*; Shafaat, et al. *(25)*).

In the current study, the tangential forces acquired during rubbing with the NiAl-hBN coating at different single-pass depths and linear speeds are presented in Fig. 20. As an example, the rubbing stress at the largest single-pass depth of 7.107 μm and speed of 150 m/s was calculated. The tangential force was 20 N. The contact area was equal to the product of the single-pass depth and the side length of the blade tip. In particular, $s = 0.007107 \times 4 = 0.028428$ mm^2, where s was referred to as the contact area. Then, the calculated tangential stress $\sigma_t = 703.5$ mPa. Consequently, the tangential stress suffered by the blade tip was considerably higher than its flow stress when the temperature reached 1000°C. The blade tip was softened and experienced plastic flow. The 1000°C temperature was lower than the melting point of the NiAl-hBN coating; hence, the softened blade material transferred to the NiAl-hBN coating and resulted in the smear strip shown in Fig. 16.

Conclusions

The material transfer behaviors of Al-hBN and NiAl-hBN coatings rubbed by a Ti6Al4 V blade at different linear speeds and single-pass depths were studied using a high-speed rubbing test rig. The main conclusions are summarized as follows.

1. The Al-hBN material transferred to the blade tip during high-speed rubbing. The transfer resulted from the accumulation of deformed plastic and melted metal-phase Al. This process was assisted by the burning of the lubrication-phase BN.
2. The blade material transferred to the NiAl-hBN coating during high-speed rubbing, which formed a transfer/mixed layer. The blade tip was softened by high frictional heat and sheared to smear to the coating with the generation of the layered transfer/mixed layer. Oxidation occurred during the aforementioned process.
3. The attainable average temperature of the contact face when rubbed with the NiAl-hBN coating was 1.6 times that when rubbed with the Al-hBN coating because of the different thermophysical properties of the coatings. Different attainable temperatures at the contact face, melting points of the coatings, and blade plastic flow softening behavior resulted in completely different material transfer behaviors of the two coatings.

Funding

This work was funded by the National Natural Science Foundation of China (Grant No. 50675215), the Tribology Science Fund of State Key Laboratory of Tribology (Grant No. SKLTKF15B09), and Innovation Foundation of China Aviation Industry Corp. (Grant No. 2010E41018).

References

(1) Borel, M. O., Nicoll, A. R., Schläpfer, H. W., and Schmid, R. K. (1989), "The Wear Mechanisms Occurring in Abradable Seals of Gas Turbines," *Surface and Coatings Technology*, **39–40**, pp 117–126.
(2) Bill, R. C. and Shiembob, L. T. (1977), "Friction and Wear of Sintered Fibermetal Abradable Seal Materials," *Journal of Lubrication Technology*, **99**(4), pp 421–427.
(3) Stringer, J. and Marshall, M. B. (2012), "High Speed Wear Testing of an Abradable Coating," *Wear*, **294–295**, pp 257–263.
(4) Fois, N., Stringer, J., and Marshall, M. B. (2013), "Adhesive Transfer in Aero-Engine Abradable Linings Contact," *Wear*, **304**(1–2), pp 202–210.
(5) Laverty, W. F. (1982), "Rub Energetics of Compressor Blade Tip Seals," *Wear*, **75**(1), pp 1–20.
(6) Bounazef, M., Guessasma, S., and Ait Saadi, B. (2004), "The Wear, Deterioration and Transformation Phenomena of Abradable Coating BN-SiAl-Bounding Organic Element, Caused by the Friction between the Blades and the Turbine Casing," *Materials Letters*, **58**(27–28), 3375–3380.
(7) Kennedy, F. E. (1980), "Thermomechanical Phenomena in High Speed Rubbing," *Wear*, **59**(1), pp 149–163.
(8) Kennedy, F. E. and Ling, F. F. (1974), "A Thermal, Thermoelastic, and Wear Simulation of a High-Energy Sliding Contact Problem," *Journal of Lubrication Technology*, **96**(3), pp 497–505.
(9) Xue, W. H., Gao, S. Y., Duan, D. L., Liu, Y., and Li, S. (2015), "Material Transfer Behaviour between a Ti6Al4 V Blade and an Aluminium Hexagonal Boron Nitride Abradable Coating during High-Speed Rubbing," *Wear*, **322–323**, pp 76–90.
(10) Luo, H., Hao, L. P., and Wei, Z. W. (1999), "Study on the Oxidation Performance of Titanium Alloy," *Proceedings of the Ninth China Welding Conference*, Hei Longjiang, China.
(11) Rigney, D. A. and Hirth, J. P. (1979), "Plastic Deformation and Sliding Friction of Metals," *Wear*, **53**(2), pp 345–370.
(12) Uetz, H. and Föhl, J. (1978), "Wear As an Energy Transformation Process," *Wear*, **49**(2), pp 253–264.
(13) Bowden, F. P. and Tabor, D. (1954), *The Friction and Lubrication of Solids*, Oxford, UK: Clarendon Press.
(14) Archard, J. F. (1959), "The Temperature of Rubbing Surfaces," *Wear*, **2**(6), pp 438–455.
(15) Blok, H. (1963), "The Flash Temperature Concept," *Wear*, **6**(6), pp 483–494.
(16) Wang, H. G. (1996), "Criteria for Analysis of Abradable Coatings," *Surface and Coatings Technology*, **79**(1–3), pp 71–75.
(17) Chassaing, G., Pougis, A., Philippon, S., Lipinski, P., Faure, L., Meriaux, J., Demmou, K., and Lefebvre, A. (2015), "Experimental and Numerical Study of Frictional Heating during Rapid Interactions of a Ti6Al4 V Tribopair," *Wear*, **342–343**, pp 322–333.

(18) Chassaing, G., Faure, L., Philippon, S., Coulibaly, M., Tidu, A., Chevrier, P., and Meriaux, J. (2014), "Adhesive Wear of a Ti6Al4 V Tribopair for a Fast Friction Contact," *Wear*, **320**, pp 25–33.
(19) Rahaman, M. L. and Zhang, L. (2014), "On the Estimation of Interface Temperature during Contact Sliding of Bulk Metallic Glass," *Wear*, **320**(1–2), pp 77–86.
(20) Tzanakis, I., Conte, M., Hadfield, M., and Stolarski, T. A. (2013), "Experimental and Analytical Thermal Study of PTFE Composite Sliding against High Carbon Steel as a Function of the Surface Roughness, Sliding Velocity and Applied Load," *Wear*, **303**(1–2), pp 154–168.
(21) Emery, A. F., Wolak, J., Etemad, S., and Choi, S. R. (1983), "An Experimental Investigation of Temperatures Due to Rubbing at the Blade–Seal Interface in an Aircraft Compressor," *Wear*, **91**(2), pp 117–130.
(22) Zenas, R., Archbold, T., Wolak, J., Emery, A. F., and Etemad, S. (1985), "Metallurgical and Mechanical Phenomena Due to Rubbing of Titanium against Sintered Powder Nichrome," *Tribology Transactions*, **28**(1), pp 97–103.
(23) Porntadawit, J., Uthaisangsuk, V., and Choungthong, P. (2014), "Modeling of Flow Behavior of Ti-6 Al-4 V Alloy at Elevated Temperatures," *Materials Science and Engineering A*, **599**, pp 212–222.
(24) Ding, R., Guo, Z. X., and Wilson, A. (2002), "Microstructural Evolution of a Ti-6 Al-4 V Alloy during Thermomechanical Processing," *Materials Science and Engineering A*, **327**(2), pp 233–245.
(25) Shafaat, M. A., Omidvar, H., and Fallah, B. (2011), "Prediction of Hot Compression Flow Curves of Ti-6 Al-4 V Alloy in $\alpha+\beta$ Phase Region," *Materials & Design*, **32**(10), pp 4689–4695.
(26) Carslaw, H. and Jaeger, J. (1959), *Conduction of Heat in Solids*, 2nd ed., Oxford, UK: Clarendon Press.
(27) Jaeger, J. C. (1942), "Moving Sources of Heat and the Temperature of Sliding Contacts," *Proceedings of the Royal Society of New South Wales*, **76**, pp 203–224.
(28) Archard, J. F. and Rowntree, R. A. (1988), "The Temperature of Rubbing Bodies; Part 2, the Distribution of Temperatures," *Wear*, **128**(1), pp 1–17.
(29) Bowden, F. P. and Thomas, P. H. (1954), "The Surface Temperature of Sliding Solids," *Proceedings of the Royal Society A – Mathematical and Physical Sciences*, **223**(1152), pp 29–40.
(30) Tian, X. and Kennedy, F. E. (1994), "Maximum and Average Flash Temperatures in Sliding Contacts," *Journal of Tribology*, **116**, pp 167–174.

Appendix. Estimation of temperature in the contact area

Carslaw and Jaeger *(26)* and Jaeger *(27)* obtained the formulas for the maximum and average flash temperatures on the contact surfaces of sliding friction based on heat conduction theories and through complex mathematical derivations. The average flash temperature referred to is the average of the flash temperatures over the entire contact area. Its value is equal to the result of the maximum flash temperature multiplied by a constant less than 1. Archard *(14)* and Archard and Rowntree *(28)* omitted the mathematical complexities of Jaeger *(27)* and Blok's *(15)* theories and instead emphasized physical considerations upon which calculations were based; he obtained the formula for the average flash temperature. The following discussion begins with a brief introduction of the theory of Jaeger *(27)* and Archard. *(14)* Then, the theory is applied in studying the considerable differences in wear behaviors presented by the two coatings, with the help of other studies on flash temperature.

A sliding friction pair based on Archard's theory *(14)* is shown in Fig. A1. Body B moves with a velocity V over the flat surface of body C. A circular contact area with radius a was formed. Let Q_b be the quantity of heat supplied per second to body B and Q_c be the quantity of heat supplied per second to body C. The thermal conductivity and thermal diffusivity of body B were K_B and χ_B, respectively. Accordingly, K_C and χ_C were used for body C.

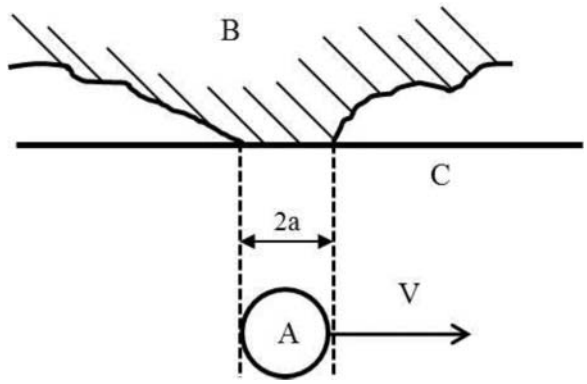

Figure A1. Schematic diagram of the sliding friction pair.

For body B, heat was supplied to a fixed area and a steady-state condition was achieved. Through comparison with the corresponding electrical problem, the average temperature was obtained as

$$\theta_{mB} = \frac{Q_B}{4aK_B}. \qquad [A1)]$$

For body C, when the sliding speed V of body B was small, such that sufficient time for steady heat conduction was established at each position of the contact area in body C, then, by analogy with Eq. [1], the average temperature was

$$\theta_{mC} = \frac{Q_C}{4aK_C}. \qquad [A2]$$

When speed V was sufficiently large, such that the contact time between bodies B and C was considerably less than the required time to establish steady heat conduction, Eq. [2] was no longer available. Under this condition, Jaeger *(27)* used the dimensionless quantity L to distinguish between low- and high-speed conditions.

$$L = \frac{Va}{2\chi_C}. \qquad [A3]$$

When $L < 0.1$, Eq. [2] was available. When $L > 5$, other formulas should be applied. However, Jaeger *(27)* did not provide the physical significance of L. Archard's *(14)* discussion on the physical significance of L in terms of heat penetration depth into the bulk of the contact material is widely accepted.

On the basis of Archard's *(14)* mathematical derivation, L is equal to the ratio of the heat penetrating time to depth a to contact time. L increased with the increase in sliding speed V, and heat affected the increase in depth. This assumption was proven via a simple experiment conducted by Blok *(15)*. A torch was made to travel at a uniform speed over a bright sheet of steel. The higher the speed, the narrower the band of annealing colors, which indicated that the heat penetration depth decreased.

From the preceding discussion, when L was extremely large, the heat penetration depth was too small compared with the

contact radius. Hence, the sideways flow of heat could be neglected and the problem could be regarded as one of linear heat flow. When the theory of Jaeger *(27)* was used, the average temperature was

$$\theta_{mC} = \frac{2qt^{\frac{1}{2}}}{(\pi K_C \rho_C c_C)^{\frac{1}{2}}}, \quad [A4]$$

where q is the heat flux; t is the contact time; and ρ_C and c_C are the density and thermal capacity of body C, respectively. When $t = a/V$, $\chi_C = K_C/\rho_c C_c$, and $q = Q_C/\pi a^2$ were integrated into Eq. [A4] and when the rubbing speed of body B was extremely high ($L > 5$), the average temperature of body C was

$$\theta_{mC} = \frac{0.36Q_C}{K_c a}\left(\frac{\chi_C}{Va}\right)^{\frac{1}{2}}. \quad [A5]$$

Although differences were found in the constants, Eq. [A5] was in accordance with the equations proposed by other researchers (Blok *(15)*; Jaeger *(27)*; Bowden and Thomas *(29)*; Tian and Kennedy *(30)*). However, a problem lay in the application of these equations because the proportion of frictional heat supplied to each of the two rubbing bodies was not determined. Numerous studies were conducted to solve the problem.

Jaeger *(27)* assumed that when a steady state of heat conduction had been attained, a fraction ζ of the heat flux q passed to body C and the remaining fraction $1 - \zeta$ moved to body B. With the temperature calculated with the deduced equation for body C with a moving heat source equal to the temperature calculated for body B with a stationary heat source, fraction ζ was determined by Jaeger *(27)*. When the sliding speed was high,

$$\zeta = \frac{K_C V^{\frac{1}{2}}}{K_C V^{\frac{1}{2}} + 1.504(\chi_C K_B \sigma)^{\frac{1}{2}}}, \quad [A6]$$

in which σ is the emissivity of body B. It can be seen from Eq. [A6] that as the linear speed V increased, the frictional heat that passed to body C increased.

Following Jaeger *(27)*, ζ could also be deduced from Eq. [1] and Eq. [A5], which is

$$\zeta = \frac{K_C V^{\frac{1}{2}}}{K_C V^{\frac{1}{2}} + 1.44K_B(a\chi_C)^{\frac{1}{2}}}. \quad [A7]$$

Equation [A7] gives the same conclusion as Eq. [A6].

In addition, for the distribution fraction of frictional heat, Tian and Kennedy *(30)* proposed a calculation formula based on Blok's *(15)* theory; that is,

$$\zeta = \frac{1}{1 + \frac{K_B}{K_C}\sqrt{\frac{1+L_B}{1+L_C}}}, \quad [A8]$$

where $L_B = V_c a/2\chi_B$ and $L_C = V_B a/2\chi_C$. Again, when the sliding speed V of body B was extremely high, most of the frictional heat passed to body C. During high-speed sliding, the fraction of frictional heat passing to the physically motionless body C with a moving heat source increased with an increase in sliding speed (Bowden and Thomas *(29)*).